Computational Materials Science 155 (2018) 400–409

Contents lists available at ScienceDirect

Computational Materials Science

journal homepage: www.elsevier.com/locate/commatsci

New mechanisms of helical dislocation formation via the pinch-off process near a nano-inhomogeneity

Yi Cui[a,*], Zengtao Chen[b], Yang Ju[a]

[a] Department of Mechanical Science & Engineering, Graduate School of Engineering, Nagoya University, Nagoya 464-8603, Japan
[b] Department of Mechanical Engineering, University of Alberta, Edmonton, AB T6G 2G8, Canada

ARTICLE INFO

Keywords:
Helical dislocation
Pinch-off
Shear dislocation loop
Prismatic dislocation loop
Cross-slip

ABSTRACT

Early experiments showed that short helical dislocations can be generated near an inhomogeneity in crystal materials under hydrostatic loading. For the first time, atomistic simulations also reveal that a nano-inhomogeneity can not only induce rows of prismatic loops but also helical dislocations under hydrostatic loading. Two new mechanisms of helical dislocation formation are discovered via molecular dynamics (MD) simulations. Both concern the pinch-off process between dislocation segments. The first mechanism is the pinch-off failure of an unclosed prismatic loop. The second mechanism is the early pinch-off between two nested, cross-slipped shear loops before evolving into prismatic ones. The configuration of the two closing-in dislocation segments is crucial. Two screw segments with opposite line directions will feel a strong attractive force, while other configurations may not. Thus, the pinch-off process is either promoted or hindered. The reduction of screw components can be viewed as a need to lower the interaction energy between dislocation loops. The stress required to sustain the formation of dislocation helix is found much lower than that needed to trigger dislocation emission. In addition to the formation mechanism, the ongoing material transport is studied and its distribution is revealed concerning the helical turns. To our best knowledge, the formation of helical dislocations near a nano-inhomogeneity in an initially dislocation-free matrix has never been studied via atomistic simulations.

1. Introduction

The formation of geometrically-necessary dislocations such as prismatic loops and shear loops under high-strain-rate loading have been extensively studied and well-understood [1–4]. Under hydrostatic loading, prismatic loops can be generated and detached from void, causing its growth [2]. A prismatic loop can also be formed by a shear loop through cross-slipping and pinching off of screw components in a "lasso" action [3]. Aside from this "lasso" style pinch-off, a new pinch-off mechanism to create prismatic loop out of two nested shear loops was reported recently [4]. In contrast, the formation of helical dislocations from nano-inhomogeneities due to the pinch-off behavior between dislocation segments has never been reported. The current understanding from atomistic simulations is that helical dislocations can originate from straight screw dislocations. Regarding this, molecular dynamics simulations have been employed to explore the formation mechanism of helical dislocations from straight screw dislocations in both FCC [5] and BCC [6] crystals, due to the interaction with either Frank loops or self-interstitial clusters. Under hydrostatic loading, precipitation can induce not only prismatic loops but also short helical dislocations as seen in Fig. 1. However, such formation of helical dislocations due to nano-inhomogeneities has never been reported via molecular dynamics simulations. On the other hand, continuum-based simulations can be a powerful tool to investigate the pertinent structure of prismatic dislocations [7] or even dislocation helix structure. Their merit is that they can handle much longer time scale than can the molecular dynamics, yet they rely on the material or dislocation models that usually omit the full atomic structure. The tradeoff between high efficiency and fidelity appears inevitable. In this regard, molecular dynamics can readily capture full atomic displacements, which cannot be easily reflected by continuum-based simulations, although the time scale may not be sufficient to cover long-term diffusion phenomenon. It should be underscored that (1) the surface cut to create a dislocation can be arbitrary [8] and (2) the displacement for a given distribution of dislocations is not a state quantity, which rather depends on the history of creation [9]. The removal or insertion of material can be viewed as both a consequence of geometrically-necessary dislocations [1] and a requirement for their generation [8]. Mass transfer due to helical dislocations can also generate certain types of whiskers on crystal surfaces [10]. Recently, nanowire and nanotube growth facilitated by axial

* Corresponding author.
E-mail address: cui7@ualberta.ca (Y. Cui).

https://doi.org/10.1016/j.commatsci.2018.08.063
Received 5 August 2018; Accepted 29 August 2018

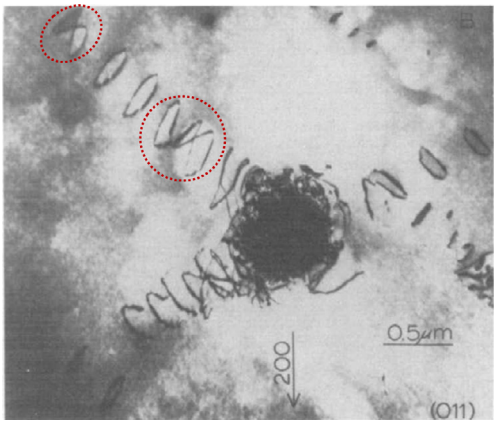

Fig. 1. Helical dislocations (marked by red circles) observed in Ref. [12] (Reprinted with permission from Makenas et al. 1980. Copyright 1980 Elsevier). (For interpretation of the references to colour in this figure legend, the reader is referred to the web version of this article.)

screw dislocations was revealed [11]. Since screw dislocations lead to helical dislocations when pinned or interacted with other defects [5,6,10], the understanding of helical dislocation generation and its mass transfer not only concerns the plastic behavior but also may provide new insights into dislocation-mediated deformation and nanofabrication.

2. Simulation setup

The molecular dynamics simulation here was performed by the Large-scale Atomic/Molecular Massively Parallel Simulator (LAMMPS) [13]. The atomic interaction is modeled by the modified embedded atom method (MEAM) [14,15]. The total energy E of a system is approximated as the sum of the atomic energies [15]:

$$E = \sum_i \left[F_i(\bar{\rho}_i) + \frac{1}{2}\sum_{j\neq i} \phi_{ij}(r_{ij}) \right], \quad F_i(\bar{\rho}_i) = \begin{cases} A_i E_i^0 \bar{\rho}_i \ln(\bar{\rho}_i) & \bar{\rho}_i \geqslant 0 \\ -A_i E_i^0 \bar{\rho}_i & \bar{\rho}_i < 0 \end{cases} \tag{1}$$

where F_i is the embedding function, $\bar{\rho}_i$ is the background electron density at the site of atom i, $\phi_{ij}(r_{ij})$ is the pair potential between atoms, E_i^0 is the sublimation energy and the parameter A_i depends on the element type of atom i. The background electron density $\bar{\rho}_i$ takes the form

$$\bar{\rho}_i = \begin{cases} \rho_i^{(0)}\sqrt{1+\Gamma_i}/\rho_i^0 & \Gamma_i \geqslant -1 \\ -\rho_i^{(0)}\sqrt{1+\Gamma_i}/\rho_i^0 & \Gamma_i < -1 \end{cases}, \quad \Gamma_i = \sum_{k=1}^{3} t_i^{(k)} \left(\frac{\rho_i^{(k)}}{\rho_i^{(0)}} \right)^2 \tag{2}$$

where ρ_i^0 is the composition-dependent electron density scaling, $t_i^{(k)}$ is the average weighting factors, $\rho_i^{(0)}$, $\rho_i^{(0)}$, $\rho_i^{(0)}$ and $\rho_i^{(0)}$ are the zeroth and higher-order densities given in [15]. Unlike the embedded atom method (EAM), the electron densities in MEAM depend on the displacement vector rather than only the scalar distance between atoms. Unlike the EAM potential, the electron densities in MEAM depend on the displacement vector rather than only the scalar distance between atoms. Jelinek et al. [15] improved the previous MEAM parameters [14] for better agreement with generalized stacking fault energies. Their new MEAM potentials were validated towards the density functional theory (DFT), classical MD (CMD) and experimental results. As a physical simplification, a periodic cubic simulation box is created to represent uniformly-distributed nano-inhomogeneities inside an infinite matrix (see Fig. 2 and Table 1). Energy minimization using a conjugate gradient algorithm is performed, followed by the relaxation step to reach an equilibrium-state configuration. The relaxation is performed at 100 K with zero external stress via the Nose-Hoover thermostat and barostat [16,17]. The adopted equilibrium duration is 20 ps [18,19]. Based on the relaxed configuration, a load of engineering tensile strain rate of $5e8s^{-1}$ is applied in all three directions. No thermostat or barostat is activated during loading. For the equal triaxial tension, lattice orientation appears less important due to symmetry. The orientations [1 0 0], [0 1 0] and [0 0 1] are aligned with the x, y and z directions, respectively for the FCC copper and the diamond-structure silicon particle if embedded. According to simulations with the same MEAM potential and other EAM potentials, dislocation formation appears insensitive to the strain rate concerned [19,20] and even irregularity in the initial shape of nanovoid [21]. Our MD data is post-processed and plotted by the software ATOMVIEWER [22].

3. Results and discussion

3.1. Characterization of the dislocation network

In defective anisotropic crystal materials, shear stress on a certain slip plane can be large enough to offset the attraction from a void [1]. Incipient shear loops therefore emerge near the void surface and continuously evolve, as revealed by the simulation. During the development of the dislocation structure, two kinds of dislocation reactions prevail. The first kind of reaction forms the Hirth lock such as those red short dislocations in Fig. 3:

$$1/6[1\bar{1}2] + 1/6[11\bar{2}] \rightarrow 1/3[100] \tag{3}$$

The second kind of reaction is the dissociation of a perfect dislocation into two Shockley partials:

$$1/2[101] \rightarrow 1/6[1\bar{1}2] + 1/6[211] \tag{4}$$

In term of helical dislocation formation, simulation size matters. For the simulation cases 1–4 with relative small size, only prismatic dislocations are generated from incipient shear loops. For the simulation case 5, a detached, eight-shape helical dislocation is observed in Fig. 3, which quite resembles that in Fig. 1 from an early experiment. A total of 12 rows of prismatic/helical dislocations are marked by arrows in Fig. 3, which resemble the punched-out “dislocation rosette” observed in low-dislocation-density copper [23]. Most rows have only developed one detached prismatic loop in Fig. 3. Only one row has so far emitted two consecutive prismatic loops. The zoom-in configuration of the detached helical dislocation in the simulation case 5 is plotted in Fig. 4(a). For the simulation case 7 with a silicon particle embedded instead of a void, a single, undetached helical dislocation is spotted and is displayed in Fig. 4(b). The first two helical dislocations are identical in term of their formation mechanism. For the simulation case 6 with the largest system size, four helical dislocations are found attached to the void surface. Among them, we present the one that has been formed differently compared to the former two. Judging from the increasing count of the helical dislocations with the increasing simulation size, more spacing seems to facilitate the formation of helical dislocations. Yet, an in-depth examination on this issue will be non-trivial and hence beyond the scope of this study.

Three typical helical dislocations are shown in Fig. 4. The pitch λ of the helix is measured as the distance between similar structures of the two turns. For the three helical dislocations, the pitch λ is found to be 7.85 nm, 7.22 nm and 8.90 nm, respectively. Since the cross-section of the glide cylinder is a rhomb instead of a circle, the radius is measured as the average distance towards the center axis along the helix. The radius is measured as 3.81 nm, 4.46 nm and 3.61 nm, respectively for the three helices. The first two are averaged along the two helical turns, while the last one is averaged along the only turn that it has so far completed. These geometry parameters are required for the stress estimation below. The Thompson tetrahedron notion is applied along each helix and the orientation of the tetrahedron is shown as inset. According to the assigned sense of line direction, the parallel segments in neighboring turns share the same direction. In Fig. 4, the dislocation reaction in the acute corner to form the short red segments can be